Hanle effect in nonmonochromatic laser light

R. E. Ryan* and T. H. Bergeman
State University of New York at Stony Brook, Stony Brook, New York 11794
(Received 15 October 1990)

We report results of calculations on the Hanle effect in a $J=0\leftrightarrow J=1$ atomic transition with three types of model fluctuating light fields: (a) the Brownian-motion phase-diffusion field, as produced in recent experiments by Arnett *et al.* [Phys. Rev. A **41**, 2580 (1990)]; (b) Gaussian amplitude fluctuations; and (c) the chaotic field model, in which real and imaginary parts of the electric-field amplitude fluctuate. For the stochastic density-matrix equations, we use methods developed by Zoller and co-workers [e.g., Dixit, Zoller, and Lambropoulos, Phys. Rev. A **21**, 1289 (1980)] employing the Fokker-Planck operator and leading to matrix continued-fraction expansions. The Hanle effect is of interest as a prototype for multisublevel atomic transitions. The width of the Hanle dip at zero magnetic field reflects the tendency of the light field to preserve the coherence between excited-state sublevels. For monochromatic light, the Hanle dip width increases as the square root of light intensity. When the laser bandwidth increases, power broadening of the coherence dip normally decreases. However, with the Brownian-motion phase-diffusion model, if the laser spectral profile is nearly Gaussian, broadening the laser up to several times the natural width of the atomic line does not diminish the Hanle dip width. With amplitude fluctuations, even in the limit of monochromatic light, power broadening of the Hanle dip with intensity is reduced by one-third to one-half depending on the particular model.

I. INTRODUCTION

Recently there has been renewed interest in understanding atomic processes induced by laser light that is not monochromatic, but has a bandwidth comparable to the linewidth of the atomic transition of interest. Atomic excitation either by broadband or by monochromatic light is well understood in terms of rate equations or Bloch equations, respectively. Considerable effort has now been expended to fill the gap between these limiting cases so as to provide a comprehensive theory of laser excitation. The recent renewal of interest stems from the development of experimental laser modulation techniques[1,2] that produce well-characterized light with the properties of idealized models. After earlier experiments on two-photon processes,[3,4] experiments on the Hanle effect in Yb have been performed[5] with a range of laser intensities. In the present report, we show how the methods for solving stochastic density-matrix differential equations developed largely by Zoller and co-workers[6–10] were applied to these Hanle effect experiments. We present results for a wider range of laser parameters than was used by Arnett *et al.*,[5] and also apply similar computational methods to other models in which the amplitude, rather than the phase, fluctuates.

When the laser field is sufficiently intense that many photon interactions occur, the laser spectral bandwidth or spectral shape, obtained from the second-order correlation function, is inadequate to characterize the field. Rather than using higher-order correlation functions explicitly, as in most discussions of finite-bandwidth effects we employ soluble models for fluctuating light fields. The Brownian-motion phase-diffusion model (BMPDM), the Gaussian amplitude model (GAM), and the chaotic field model (CFM) are considered in parallel with a discussion on two-level atom transitions by Georges.[11] (The BMPDM is a more general phase-diffusion model than Georges discussed.) Techniques for experimentally producing laser light obeying the BMPDM were developed by Elliott, Roy, and Smith.[1,2] Recently, Elliott and coworkers have produced GAM (Ref. 12) and CFM (Ref. 13) fields by modulation of monochromatic laser light. Hence it is now possible to test experimentally the theoretical predictions for each of these model fields.

The Hanle effect[14] is of interest as a prototype for transitions between multisublevel atomic states because the coherence between excited-state sublevels plays a crucial role. For a $J=0\leftrightarrow J=1$ transition, if the linear polarization of the exciting light (taken to be along x) and the direction of observation are parallel, the observed fluorescence signal is zero at zero magnetic field because fluorescent transitions from the $m_J=\pm 1$ sublevels destructively interfere. The level scheme and typical experimental geometry are shown in Fig. 1. When a z-directed magnetic field is applied, the two $m_J=\pm 1$ sublevels no longer evolve at the same frequency, the induced polarization precesses, and the observed fluorescence signal increases. If the excitation is narrow band, the fluorescence eventually decreases due to detuning as the levels separate in the magnetic field. The case of monochromatic excitation was considered theoretically by Avan and Cohen-Tannoudji[15] and observed experimentally with low intensity relative to saturation by Rasmussen, Schieder, and Walther.[16] The Hanle dip at zero field broadens with increasing intensity because the stimulated emission and reexcitation partially preserve the coherence between the upper sublevels. The ability of an intense laser to preserve coherence between the $m_J=\pm 1$ excited-state sublevels depends on the laser bandwidth and statistics. The experiments of Arnett *et al.*[5] showed power

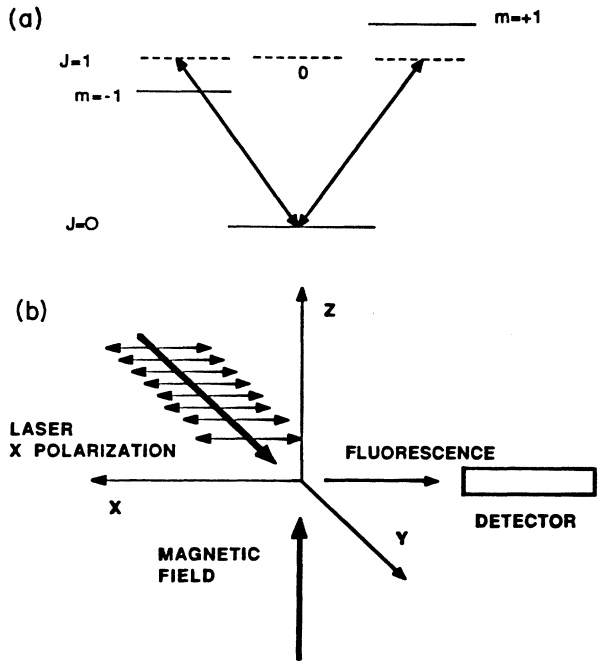

FIG. 1. (a) Energy-level diagram for the Hanle effect in a $J=0\leftrightarrow J=1$ atomic transition. (b) Schematic diagram of the typical experimental geometry for experiments discussed here.

broadening of the Hanle dip in monochromatic light, and decreased broadening with increasing laser bandwidth for Lorentzian laser profiles. There were also data showing that a more Gaussian profile produces more power broadening than a Lorentzian profile of the same bandwidth. Basic, qualitative physical explanations were given in Ref. 5. Our goal here is to show how methods for solving stochastic differential equations may be used to calculate signals for the Hanle effect for amplitude as well as phase fluctuations. A primary focus will be the extent to which the coherence between the excited-state sublevels is preserved in nonzero magnetic field (as shown by the width of the Hanle dip) in an intense laser field as the laser bandwidth increases due to various types of fluctuations.

The effects of phase and/or amplitude fluctuations on the Hanle signal may be compared with analogous effects that occur in other atomic excitation processes. One early theoretical conclusion, not yet confirmed experimentally, was that Mollow sidebands in resonance fluorescence would be quickly washed out with amplitude fluctuations, but much less so with phase fluctuations.[17] In optical double resonance with a strong saturating field and a weak probe field, the doublet split by the Rabi frequency has been observed to exhibit the predicted reversal of intensity asymmetry for a Lorentzian exciting profile.[3] In two-photon excitation, the absorption linewidth relative to the laser width with a Lorentzian laser spectral profile was observed to be twice that with a nearly Gaussian laser profile,[4] in accord with theoretical predictions. Also, in the microwave region, a Gaussian noise source has been used to modulate oscillator output to produce comparable effects.[18] Recently, the variance of fluorescence intensity as a function of laser detuning has also been shown to depend sensitively on laser phase fluctuations.[19]

Theoretical models of fluctuating narrow-band optical fields applied to atomic transitions date from Burshtein's solution of the excitation of a two-level atom in a Lorentzian wave with random phase jumps.[20] Agarwal[21] has discussed the Hanle effect and other atomic processes for a model light field with a Wiener-Levy-type phase diffusion, which results in atomic density-matrix equations identical with those obtained with the phase-jump model. Avan and Cohen-Tannoudji addressed the more general problem of two-level atomic excitation[22] and the Hanle effect[23] in the presence of laser with both rapid fluctuations and a slow diffusion, as in Brownian motion. However, they solved the stochastic equations only in the limit of a Rabi frequency greater than the bandwidth of the light. A short time later, Dixit, Zoller, and Lambropoulos[10] applied techniques for solving stochastic differential equations using the Fokker-Planck operator to density-matrix equations for laser excitation. This BMPDM covers the range from the Wiener-Levy PDM with short correlation times and Lorentzian spectral profile to long correlation times and a Gaussian profile. For a two-level atom, this approach leads to equations identical with those obtained by Georges[11] using eigenfunctions of the conditional averaging integral, but appears to be easier to extend to multilevel problems. Prior to the present work, neither approach was applied to the Hanle effect.

Other stochastic laser field models and methods should also be noted. The random telegraph model (RTM) seems to be quite flexible and relatively easy to apply,[24] and RTM phase fluctuations have now been produced electronically in the optical[25] and in the microwave[26] regime. Jump models for phase fluctuations have been generalized to include non-Markovian processes, and solved by integral equations.[27] For the case of correlated amplitude and phase fluctuations, the detuned-rotating-wave van der Pol oscillator model (DRWVPOM) has also been applied to two-level atomic transitions,[28] and in place of solving stochastic differential equations by eigenfunction techneques, Monte Carlo numerical simulation has been used.[27,29] It is obviously advantageous to have a variety of models, methods, and measurements to explore different possibilities.

This paper is organized as follows. In Sec. II the density-matrix equations for the Hanle effect are obtained in forms suitable for application to the laser field models. In Sec. III, the BMPDM, GAM, and CFM are discussed in more detail. The method for solving stochastic differential equations in terms of marginal averages is reviewed in Sec. IV. Some analytic results for the Hanle effect with PDM laser fields are given in Sec. V, and in Sec. VI more general numerical results are presented. Possible extensions of this work are discussed in the conclusion (Sec. VII).

II. DENSITY-MATRIX EQUATIONS FOR THE HANLE EFFECT

The typical experimental geometry for the Hanle effect in a $J=0\leftrightarrow J=1$ transition involves mutually orthogonal directions for the polarization of the exciting light, the polarization of the observed fluorescent light, and a magnetic field along the axis of quantization (see Fig. 1). Under these conditions (which correspond to the experimental configuration of Ref. 5), the Liouville equation for the density matrix,[15]

$$\dot{\sigma}=-i[H,\sigma]+\ldots , \tag{1}$$

where the ellipsis represents decay terms, involves only the ground state, denoted by the subscript 0, and the $M_J=\pm 1$ upper state levels, denoted by $\pm$ subscripts:

$$\sigma=\begin{bmatrix}\sigma_{++} & \sigma_{+-} & \sigma_{+0}\\ \sigma_{-+} & \sigma_{--} & \sigma_{-0}\\ \sigma_{0+} & \sigma_{0-} & \sigma_{00}\end{bmatrix} \tag{2}$$

with $\mathrm{Tr}(\sigma)=1$. With the experimental geometry given above, the Hanle signal is[15,23]

$$S=\sigma_{++}+\sigma_{--}-\sigma_{+-}-\sigma_{-+} . \tag{3}$$

We consider a linearly polarized laser field of the form

$$E(t)=E_0(t)\cos[\omega_c t+\phi(t)] \tag{4}$$

where ω_c is the center frequency of the laser. For the BMPDM, $E_0(t)$ is a constant and $\phi(t)$ is a stochastic variable (see below). For the GAM and CFM, $\phi(t)$ is a constant which may be taken equal to zero, and $E_0(t)$ is stochastic. The atomic frequency interval will be designated ω_0 and the Zeeman shift by ω_z (both in rad/sec), where $\hbar\omega_z=g\mu_0 B$, in terms of the g factor, the Bohr magneton μ_0, and the applied magnetic field. We define the Rabi frequency for a multilevel transition as the amplitude E_0 of the applied field times the reduced dipole moment element $|\mu|$ divided by $\hbar$. In a $J=0\leftrightarrow J=1$ transition (Fig. 1), each of the sublevel transition elements, $\mu_{\pm 0}$, happens to be equal to $|\mu|$, since each upper sublevel has only one decay branch. For an x-polarized field, the amplitude of the σ^+ component is $2^{-1/2}$ times E_0, while the $\exp(i\omega_c t)$ term in (4) involves another factor 2^{-1}. Hence in the Hamiltonian we will use the quantity $v(t)$, related to $\omega_R(t)$ by

$$\omega_R(t)=\frac{|\mu|E_0(t)}{\hbar}=2\sqrt{2}v(t) . \tag{5}$$

To simplify the notation, the parameter $v=v(t)$ will be used as the stochastic variable in the discussion of amplitude fluctuations. With these definitions, neglecting the nonresonant component of the field, the Hamiltonian is

$$H=\begin{bmatrix}\omega_0+\omega_z & 0 & v^*\exp[-i(\omega_c t+\phi)]\\ 0 & \omega_0-\omega_z & v^*\exp[-i(\omega_c t+\phi)]\\ v\exp[i(\omega_0 t+\phi)] & v\exp[i(\omega_c t+\phi)] & 0\end{bmatrix} \tag{6}$$

where the possible time dependence of v and ϕ is not explicit. Oscillations at the laser center frequency in the density-matrix elements are removed by the substitutions

$$\begin{aligned}&\sigma_{0\pm}\exp[-i(\omega_c t+\phi)]=\rho_{0\pm},\quad \sigma_{\pm\pm}=\rho_{\pm\pm} ,\\ &\sigma_{\pm 0}\exp[i(\omega_c t+\phi)]=\rho_{\pm 0},\quad \sigma_{\pm\mp}=\rho_{\pm\mp} .\end{aligned} \tag{7}$$

For the phase-diffusion model, it is convenient to use the following linear combinations of density-matrix elements:

$$\begin{aligned}&\psi_1=\rho_{++} ,\\ &\psi_2=\rho_{--} ,\\ &\psi_3=\rho_{+-}+\rho_{-+} ,\\ &\psi_4=i(\rho_{-+}-\rho_{+-}) ,\\ &\psi_5=\rho_{+0}+\rho_{0+} ,\\ &\psi_6=i(\rho_{+0}-\rho_{0+}) ,\\ &\psi_7=\rho_{-0}+\rho_{0-} ,\\ &\psi_8=i(\rho_{-0}-\rho_{0-})\end{aligned} \tag{8}$$

to obtain a set of equations with real coefficients:

$$\begin{aligned}&\dot{\psi}_1+\Gamma\psi_1-v\psi_6=0 ,\\ &\dot{\psi}_2+\Gamma\psi_2-v\psi_8=0 ,\\ &\dot{\psi}_3+\Gamma\psi_3-2\omega_z\psi_4-v\psi_6-v\psi_8=0 ,\\ &\dot{\psi}_4+\Gamma\psi_4+2\omega_z\psi_3+v\psi_7-v\psi_5=0 ,\\ &\dot{\psi}_5+(\Gamma/2)\psi_5+(\omega_z-\Delta-\omega)\psi_6+v\psi_4=0 ,\\ &\dot{\psi}_6+(\Gamma/2)\psi_6+(\Delta+\omega-\omega_z)\psi_5+4v\psi_1+2v\psi_2+v\psi_3=2v ,\\ &\dot{\psi}_7+(\Gamma/2)\psi_7-(\Delta+\omega+\omega_z)\psi_8-v\psi_4=0 ,\\ &\dot{\psi}_8+(\Gamma/2)\psi_8+(\Delta+\omega+\omega_z)\psi_7+4v\psi_2+2v\psi_1+v\psi_3=2v .\end{aligned} \tag{9}$$

In these equations, Γ is the natural radiative decay rate of the atomic transition, $\Delta=\omega_c-\omega_0$ is the laser detuning, and $\omega=\omega(t)=\dot{\phi}(t)$ is the stochastic component of the laser frequency.

For amplitude fluctuations, the occurrence of the sto-

chastic variable v on the right-hand side (the inhomogeneous term) complicates the approach to stochastic differential equations used here. Therefore we define an alternative set of linear combinations of density-matrix elements for which ψ_1 and ψ_2 are

$$\begin{aligned}\psi_+ &= \rho_{++}-\rho_{00}=2\rho_{++}+\rho_{--}-1\ ,\\ \psi_- &= \rho_{--}-\rho_{00}=\rho_{++}+2\rho_{--}-1\ ,\end{aligned} \tag{10}$$

and ψ_i, $i=3,\ldots,8$ are as defined in (8). The density-matrix equations for the amplitude fluctuation model then are (ω is now zero)

$$\begin{aligned}&\dot{\psi}_+ +\Gamma\psi_+ -2v\psi_6 - v\psi_8 = -\Gamma\ ,\\ &\dot{\psi}_- +\Gamma\psi_- - v\psi_6 - 2v\psi_8 = -\Gamma\ ,\\ &\dot{\psi}_3 +\Gamma\psi_3 - 2\omega_z\psi_4 - v\psi_6 - v\psi_8 = 0\ ,\\ &\dot{\psi}_4 +\Gamma\psi_4 + 2\omega_z\psi_3 + v\psi_7 - v\psi_5 = 0\ ,\\ &\dot{\psi}_5 +(\Gamma/2)\psi_5 +(\omega_z-\Delta)\psi_6 + v\psi_4 = 0\ ,\\ &\dot{\psi}_6 +(\Gamma/2)\psi_6 +(\Delta-\omega_z)\psi_5 + 2v\psi_+ + v\psi_3 = 0\ ,\\ &\dot{\psi}_7 +(\Gamma/2)\psi_7 -(\Delta+\omega_z)\psi_8 - v\psi_4 = 0\ ,\\ &\dot{\psi}_8 +(\Gamma/2)\psi_8 +(\Delta+\omega_z)\psi_7 + 2v\psi_- + v\psi_3 = 0\ .\end{aligned} \tag{11}$$

The method for solving stochastic differential equations of the form (9) or (11) is discussed below.

For the chaotic field model, v is complex, and v and v^* are both stochastic variables. In this case, it will be convenient to work with the set of density-matrix elements ρ_{ij} defined in Eq. (7), with $\psi_\pm$ from Eq. (10) instead of $\rho_{\pm\pm}$. The eight-independent equations obtained from (1) may then be written

$$\begin{aligned}&\left[\frac{d}{dt}+\Gamma\right]\psi_\pm - 2i(v\rho_{\pm 0}-v^*\rho_{0\pm}) - i(v\rho_{\mp 0}-v^*\rho_{0\mp}) = -\Gamma\ ,\\ &\left[\frac{d}{dt}+\Gamma+2i\omega_z\right]\rho_{\pm\mp} - i(v\rho_{\pm 0}-v^*\rho_{0\mp}) = 0\ ,\\ &\left[\frac{d}{dt}+\frac{\Gamma}{2}+i(\Delta\mp\omega_z)\right]\rho_{0\pm} + iv(\psi_\pm+\rho_{\mp\pm}) = 0\ ,\\ &\left[\frac{d}{dt}+\frac{\Gamma}{2}-i(\Delta\mp\omega_z)\right]\rho_{\pm 0} - iv^*(\psi_\pm+\rho_{\pm\mp}) = 0\ .\end{aligned} \tag{12}$$

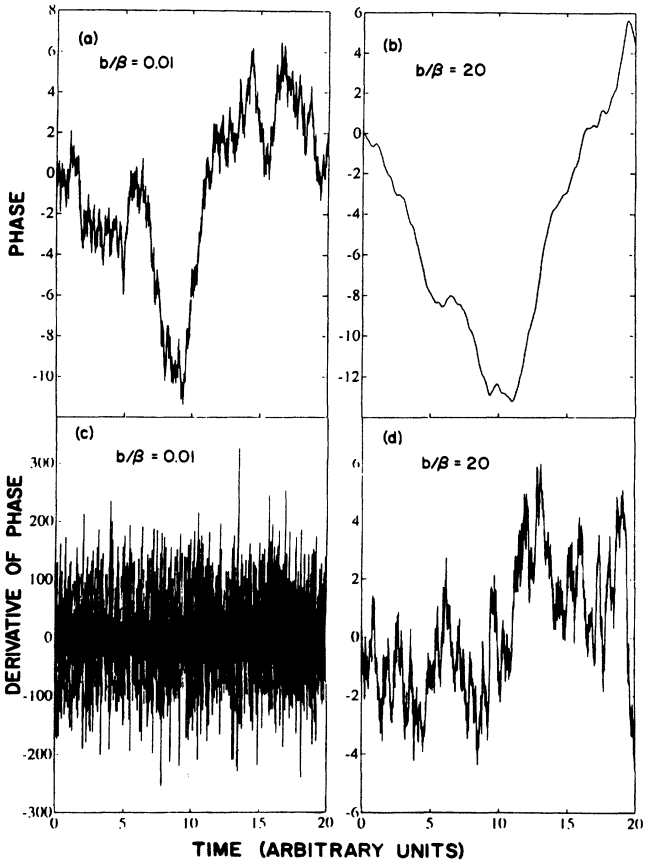

FIG. 2. Typical numerical simulations of stochastic phase and frequency in the BMPDM for a spectral width of one inverse time unit. (a) and (b) show the evolution of phase, (c) and (d) give evolution of the frequency, with parameters as indicated. The high-frequency fluctuations in (a) and (c) are associated with greater intensity in the wings of the Lorentzian as compared with Gaussian line shape.

III. MODELS OF LASER FIELDS WITH FLUCTUATIONS

A. Brownian-motion phase-diffusion model

Phase-diffusion models are closely related to the theoretical and observed properties of single mode lasers.[30–35] The amplitude of single mode lasers is stabilized due to saturation of the gain medium, and the phase diffuses due to the effects of spontaneous emission.[30–32] Semiconductor diode[33] and highly stable He-Ne (Ref. 34) lasers in fact have been shown to have Lorentzian spectral shapes out to a few linewidths from line center near

and slightly above threshold. The quantum noise or Schawlow-Townes[32] limit is usually less than a kHz for gas and dye lasers, but actual lasers are typically several orders of magnitude wider.[34,35] Therefore the spectral profile of gas and dye lasers tends to be Gaussian due to technical noise such as plasma instabilities, acoustic phenomena, and pump noise. Monolithic diode lasers, because of their short cavities, low reflectivity mirrors, and coupling between amplitude and phase noise, have quantum limit linewidths several orders of magnitude larger than gas or dye lasers, and the quantum noise regime occurs over a much larger power range.[36] Since the phase-diffusion linewidth varies inversely with power, at high power relative to threshold eventually other mechanisms also dominate the spectral linewidth and shape of diode lasers.[37]

The limiting case of instantaneous increments of ω corresponds to Wiener-Levy[38] phase diffusion which gives a purely Lorentzian spectral profile. The Brownian-motion or Ornstein-Uhlenbeck[10,38,39] phase-diffusion model assumes noninstantaneous changes in the time derivative of the phase, leading to a laser spectral density that is sub-Lorentzian in the wings. The BMPDM with finite β (e.g., finite correlation time, as defined below) provides an approximate model for lasers with non-Lorentzian profile.

As discussed by Dixit, Zoller, and Lambropoulos,[10] the stochastic variable $\omega(t)$ in the BMPDM obeys the Langevin equation for an Ornstein-Uhlenbeck process;[38–42]

$$\frac{d\omega(t)}{dt}+\beta\omega(t)=F(t) \tag{13}$$

where $F(t)$ is a δ-correlated Gaussian force:

$$\langle F(t)F(t')\rangle=2b\beta^2\delta(t-t') . \tag{14}$$

Thus $\omega(t)$ is analogous to velocity in Brownian motion, while ϕ is analogous to displacement. By integrating (13) and averaging over $F(t)$, one obtains[40–42] the correlation function for $\omega(t)$. For $t,t'\gg\beta^{-1}$

$$\langle\omega(t)\omega(t')\rangle=b\beta e^{-\beta|t-t'|} , \tag{15}$$

indicating that β^{-1} is the correlation time for $\omega(t)$, and $b\beta$ is the mean value of ω^2. In the $\beta\to\infty$ limit, corresponding to instantaneous increments of ω, the $d\omega/dt$ term in Eq. (13) may be neglected, and ϕ evolves as integrated white noise, a random walk with infinitely rapid infinitesimal steps, known as the Wiener-Levy process.[38] Noninstantaneous increments of ω occur when β is finite (the Ornstein-Uhlenbeck process).

For additional physical insight into the Brownian-motion model, we have performed numerical simulations[41] of the stochastic evolution of ϕ and ω. We integrate the Langevin equation (13) using simply the Euler method, which is adequate to show the basic features despite an error of order τ^2 per step of size τ. The noise process makes the Euler method surprisingly stable. The discrete equation is

$$\omega_{n+1}-\omega_n+\beta\omega_n\tau=\int_t^{t+\tau}F(t')dt'=(4b\beta^2)^{1/2}w_n . \tag{16}$$

$F(t)$ is a white Gaussian process, so the integral is a Gaussian process very analogous to diffusion. From (14), the diffusion constant inside the integral is $2b\beta^2$. w_n is a Gaussian random with a variance of one. The phase itself is obtained by another integration:

$$\phi_{n+1}=\phi_n+\omega_n\tau . \tag{17}$$

Figure 2(a) shows typical results for evolution of the phase with $b/\beta=0.01$, while Fig. 2(b) shows the phase for $b/\beta=20$. The corresponding plots for ω are shown in Figs. 2(c) and 2(d), respectively. A large value of β implies rapid fluctuations such that wings of the spectral distribution fall off more slowly than with a small value of β. Actually, the plots in Fig. 2 represent generic Brownian-motion behavior, with ϕ corresponding to the displacement and ω corresponding to the velocity, and as such will also be applied to the GAM discussed below.

The exact relation between b, β, and the laser spectral distribution is obtained from the Fourier transform of the correlation function,

$$\langle e^{i\phi(t+\tau)-i\phi(t)}\rangle=\exp[-b|\tau|+(e^{-\beta|\tau|}-1)/\beta] . \tag{18}$$

In the limit $\beta\to\infty$, the spectrum is Lorentzian with a width $2b$. In the limit $\beta\to0$, the spectrum is Gaussian with a width $(8b\beta\ln2)^{1/2}$. For intermediate values of b/β, we show in Fig. 3 the values of b and β that give a width $\Delta\omega_L=1$ rad/sec.

B. Gaussian amplitude model

An extreme contrast with the phase-diffusion model is presented by the Gaussian amplitude model, defined by Georges,[11] in which the (real) electric field exhibits Gaussian fluctuations about zero. It will be convenient to consider v [Eq. (5)] rather than E_0 as the stochastic variable. A Gaussian distribution of v:

$$P_0(v)=\frac{\exp(-v^2/2v_0^2)}{(2\pi)^{1/2}v_0} , \tag{19}$$

together with a value of β^{-1} for the correlation time for amplitude fluctuations, is consistent with a Langevin equation of the form (13) and (14) with the substitution

$$\beta=\frac{\Delta\omega_L}{2},\quad b\beta=v_0^2 \tag{20}$$

where $\Delta\omega_L$ is the laser bandwidth, and v_0 is the rms value of v. Figure 2 applies if we replace the label phase by amplitude. In the limit $\beta\to0$ but $b\beta$ finite, there will be a Gaussian distribution of (constant) amplitude values. Clearly this will affect the signal in a way that a distribution of phase values would not.

C. The chaotic field model

It has been shown that a laser with many uncorrelated modes may be represented by a model in which $E_0(t)$ in Eq. (4) is complex and the phase $\phi(t)$ is constant.[7–9,40] As for the GAM, we will take the coupling element v as the stochastic variable. v and v^* each obey Langevin equations of the form (13). In terms of $v_0^2=\langle|v^2|\rangle$, the stationary distribution function is

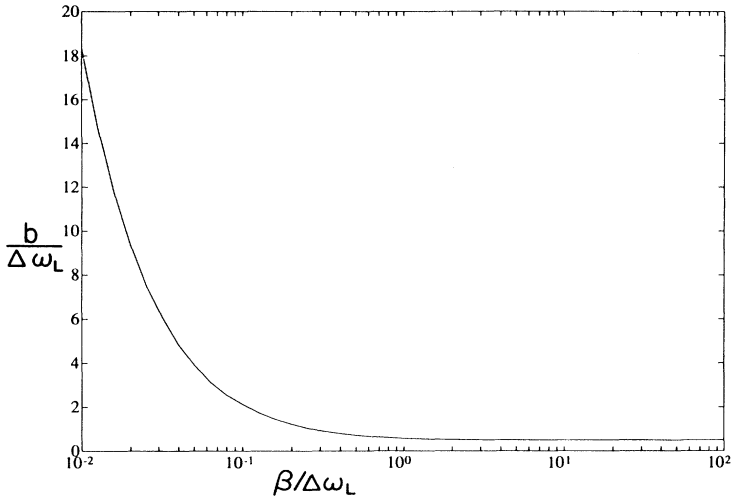

FIG. 3. Universal curve of $b/\Delta\omega_L$ vs $\beta/\Delta\omega_L$, where $\Delta\omega_L$ is the spectral FWHM, for the BMPDM. For large $\beta/\Delta\omega_L$, $b \rightarrow \Delta\omega_L/2$.

$$P_0(v,v^*)=\frac{\exp(-|v|^2/v_0^2)}{\pi v_0^2} \ . \tag{21}$$

This same distribution over laser intensity (or $|v|^2$) is obtained for thermal light arising from a large number of independent sources.[43]

IV. THE MARGINAL AVERAGES

A. PDM and GAM

The density-matrix equations (9) and (11) have the form

$$\left[\frac{d}{dt}+A+Bz\right]\psi=y \tag{22}$$

where A and B are matrices, ψ and y are vectors, and z is a stochastic variable, either $\dot{\phi}=\omega$ or v. The method followed here for solving such equations has been developed by Zoller and co-workers[6–10] and discussed also by Stenholm[40] and Risken.[41] Equations with complex z (for the CFM) will be discussed below. The density-matrix equations together with the equations for evolution of the stochastic variable z are considered to be a set of coupled Langevin equations (the stochastic force term does not occur in the equations for the density-matrix elements ψ). We recall[41] that coupled Langevin equations of the form

$$\dot{x}_i=h_i(\{x\},t)+g_i\Gamma(t) \tag{23}$$

where

$$\langle\Gamma(t)\Gamma(t')\rangle=2\delta(t-t') \tag{24}$$

lead to a Fokker-Planck equation with drift coefficients $h_i(\{x\},t)$ and diffusion coefficients g_i^2. Thus the multivariable Fokker-Planck equation for the probability distribution $P(\{x\},t)$ in this case is

$$\frac{\partial P(\{x\},t)}{\partial t}=\sum_i\left[-\frac{\partial}{\partial x_i}h_i(\{x\},t)+g_i^2\frac{\partial^2}{\partial x_i^2}\right]P(\{x\},t) \ . \tag{25}$$

For the set of variables $\{x_i, i=0-8\}$ where $x_0=z$, and $x_i=\psi_i$, $i=1-8$, we have

$$h_0=-\beta z, \quad g_0=\beta\sqrt{b} \ . \tag{26}$$

For $i=1-8$, from (22), $g_i=0$ and

$$h_i=-\sum_{j=1,8}(A_{ij}+B_{ij}z)x_j+y_i \ . \tag{27}$$

From the Langevin equation (13) for a single stochastic variable $z=\dot{\phi}$ or v, one obtains the Fokker-Planck equation

$$\frac{\partial P(z,t)}{\partial t}=\left[\beta\frac{\partial}{\partial z}z+\beta^2 b\frac{\partial^2}{\partial z^2}\right]P(z,t)=L_z P(z,t) \tag{28}$$

where L_z is the Fokker-Planck operator.

The marginal averages are obtained by integrating the probability function over the $N=8$ density-matrix elements ψ_i,

$$w_i(z,t)=\int\psi_i P(\{\psi\},z,t)d^N\psi \ . \tag{29}$$

The Fokker-Planck equation (25), with the substitutions (26) and (27), is multiplied successively by each of the ψ_i, integrated over the ψ_j, and then integrated by parts to obtain the set of equations

$$\left[\frac{\partial}{\partial t}+A+Bz-L_z\right]w(z,t)=y\bar{P}(z,t)=yP_0(z) \tag{30}$$

where w is a vector of marginal averages and

$$\bar{P}(z,t)=\int d^N\psi P(\{\psi\},z,t)=P_0(z)=\frac{\exp(-z^2/2z_0^2)}{(2\pi z_0^2)^{1/2}} \ . \tag{31}$$

The distribution function $\bar{P}(z,t)$ is time independent and equal to the Gaussian distribution $P_0(z)$. For either model,

$$z_0^2=b\beta \ . \tag{32}$$

For the Gaussian amplitude model, $z_0=v_0$ is the rms coupling element, while for the BMPDM, z_0 is the rms spread of ω.

Equation (30) for the marginal averages is solved by using an expansion in Hermite polynomials:

$$w(z,t)=\sum_n w_n(t)P_0(z)\tilde{H}_n(z) \tag{33}$$

where $\tilde{H}_n(z)$ is defined in terms of the standard Hermite polynomials $H_n(x)$:

$$\tilde{H}_n(z)=\frac{1}{(2^n n!)^{1/2}}H_n\left[\frac{z}{z_0\sqrt{2}}\right] \tag{34}$$

so that

$$\int dz\, \tilde{H}_k(z)P_0(z)\tilde{H}_n(z)=\delta_{kn} \ . \tag{35}$$

The product $P_0(z)\tilde{H}_n(z)$ is an eigenfunction of the Fokker-Planck operator L_z with eigenvalue $-n\beta$. A three-term recursion relation is obtained by substituting the series expansion for $w(z,t)$ into (30), multiplying by $\tilde{H}_k(z)$, integrating over z, and using the standard recursion relations for Hermite polynomials:

$$\left[\frac{d}{dt}+\beta n+A\right]w_n(t)+Bz_0\sqrt{n+1}\,w_{n+1}(t)+Bz_0\sqrt{n}\,w_{n-1}(t)=y_0\delta_{n,0} \ . \tag{36}$$

Here A and B are matrices, while $w_n(t)$ and y_0 are vectors. In the steady state, the time derivative and time dependencies disappear, giving a matrix recursion relation of the form

$$c_n w_n+d_n w_{n+1}+d_{n-1}w_{n-1}=y_0\delta_{n0} \ . \tag{37}$$

Methods for evaluating the continued fractions that result from such expressions are discussed in the Appendix. The desired quantity is the expectation value $\langle w(z,t)\rangle$ which in steady state is equal to w_0.

B. The chaotic field model

When both v and v^* are stochastic variables, as in (6) and (12), the Fokker-Planck operator is

$$L(v,v^*)=-b\left[\frac{\partial}{\partial v}v+\frac{\partial}{\partial v^*}v^*+2v_0^2\frac{\partial^2}{\partial v\,\partial v^*}\right] \ . \tag{38}$$

The differential equations for the marginal averages have the form

$$\left[\frac{\partial}{\partial t}+A+Bv+\bar{B}v^*-L(v,v^*)\right]w(v,v^*,t)=y\bar{P}(v,v^*,t)=y\bar{P}_0(v,v^*)=y\bar{P}_0(x)=y\exp(-x)/\pi v_0^2 \ . \tag{39}$$

We transform to "polar coordinates" $v=V\exp(i\phi)$ and introduce $x=V^2/v_0^2$. A solution of (39) may be obtained by expanding each marginal average $w_{ij}(v,v^*,t)$ in a series of the form[7-9]

$$w_{ij}(v,v^*,t)=\sum_{\alpha,n} w_{ij}^{\alpha n}(t)\bar{P}_0(x)\phi_{\alpha n}(V,\phi) \tag{40}$$

where

$$\phi_{\alpha n}=\left[\frac{n!}{(n+|\alpha|)!}\right]^{1/2}\left[\frac{V}{v_0}\right]^{|\alpha|}\exp(-i\alpha\phi)L_n^{|\alpha|}(x) \tag{41}$$

in which $L_n^{|\alpha|}(x)$ is the associated Laguerre polynomial. The $\phi_{\alpha n}$ are eigenfunctions of the Fokker-Planck operator (38):

$$L(v,v^*)\phi_{\alpha n}=b(2n+|\alpha|)\phi_{\alpha n} \ . \tag{42}$$

In obtaining recursion relations for the $w_{ij}^{\alpha n}$, the following matrix elements are needed:

$$\begin{aligned}&\langle\phi_{0n}|V\exp(\pm i\omega)|\bar{P}_0\phi_{\pm 1m}\rangle=v_0(\sqrt{n+1}\,\delta_{nm}-\sqrt{n}\,\delta_{n,m+1}) \ ,\\ &\langle\phi_{\pm 1n}|V\exp(\mp i\omega)|\bar{P}_0\phi_{0m}\rangle=v_0\sqrt{n+1}(\delta_{nm}-\delta_{n,m-1}) \ .\end{aligned} \tag{43}$$

By the same procedure used to obtain (36), Eqs. (12) for the density-matrix elements ρ_{ij} are transformed into equations for the coefficients, $w_{ij}^{\alpha n}$, in the expansion of the marginal averages. ($w_\pm$ will denote the marginal average of $\psi_\pm=\rho_{\pm\pm}-\rho_{00}$.) In the steady state

$$\begin{aligned}&(2nb+\Gamma)w_{\pm}^{0n}-2iv_0(\sqrt{n+1}\,w_{\pm 0}^{1n}-\sqrt{n}\,w_{\pm 0}^{1,n-1})+2iv_0(\sqrt{n+1}\,w_{0\pm}^{-1n}-\sqrt{n}\,w_{0\pm}^{-1,n-1})\\ &\qquad -iv_0(\sqrt{n+1}\,w_{\mp 0}^{1n}-\sqrt{n}\,w_{\mp 0}^{1,n-1})+iv_0(w_{0\mp}^{-1n}\sqrt{n+1}-\sqrt{n}\,w_{0\mp}^{-1,n-1})=-\Gamma\delta_{n0} \ ,\end{aligned} \tag{44a}$$

$$(2nb+\Gamma\pm 2i\omega_z)w_{\pm\mp}^{0n}-iv_0(\sqrt{n+1}\,w_{\pm 0}^{1n}-\sqrt{n}\,w_{\pm 0}^{1,n-1})+iv_0(\sqrt{n+1}\,w_{0\mp}^{-1n}-\sqrt{n}\,w_{0\mp}^{-1,n-1})=0 \ , \tag{44b}$$

$$[(2n+1)b+\Gamma/2+i(\Delta\mp\omega_z)]w_{0\pm}^{-1,n}+iv_0\sqrt{n+1}(w_{\pm}^{0n}-w_{\pm}^{0n+1})+iv_0\sqrt{n+1}(w_{\mp\pm}^{0n}-w_{\mp\pm}^{0,n+1})=0 \ , \tag{44c}$$

$$[(2n+1)b+\Gamma/2-i(\Delta\mp\omega_z)]w_{\pm 0}^{1,n}-iv_0\sqrt{n+1}(w_{\pm}^{0n}-w_{\pm}^{0n+1})-iv_0\sqrt{n+1}(w_{\pm\mp}^{0n}-w_{\pm\mp}^{0,n+1})=0 \ . \tag{44d}$$

Expressions for $w_{0\pm}^{-1,n}$ and $w_{\pm 0}^{1,n}$ may be obtained from the four equations represented by (44c) and (44d), and substituted into (44a) and (44b). This yields recursion relations for the four variables $w_{\pm}$ and $w_{\pm\mp}$:

$$[2nb+\Gamma+2(A_n^{\pm}+A_{n-1}^{\pm})]w_{\pm}^{0n}+(A_n^{\mp}+A_{n-1}^{\mp})w_{\mp}^{0n}+(B_n^{\pm}+B_{n-1}^{\pm})w_{\pm\mp}^{0n}+(B_n^{\pm *}+B_{n-1}^{\pm *})w_{\mp\pm}^{0n}-2A_n^{\pm}w_{\pm}^{0n+1}$$
$$-2A_{n-1}^{\pm}w_{\pm}^{0n-1}-A_n^{\mp}w_{\mp}^{0n+1}-A_{n-1}^{\mp}w_{\mp}^{0n-1}-B_n^{\pm}w_{\pm\mp}^{0n+1}-B_{n-1}^{\pm}w_{\pm\mp}^{0n-1}-B_n^{\pm *}w_{\mp\pm}^{0n+1}-B_{n-1}^{\pm *}w_{\mp\pm}^{0n-1}=-\Gamma\delta_{n0}\ , \quad (45a)$$

$$(D_n^{\pm}+D_{n-1}^{\pm})w_{\pm}^{0n}+(D_n^{\mp *}+D_{n-1}^{\mp *})w_{\mp}^{0n}+(2nb+\Gamma\pm 2i\omega_z+C_n^{\pm}+C_{n-1}^{\pm})w_{\pm\mp}^{0n}-D_n^{\pm}w_{\pm}^{0n+1}-D_{n-1}^{\pm}w_{\pm}^{0n-1}$$
$$-C_n^{\pm}w_{\pm\mp}^{0n+1}-C_{n-1}^{\pm}w_{\pm\mp}^{0n-1}-D_n^{\mp *}w_{\mp}^{0n+1}-D_{n-1}^{\mp *}w_{\mp}^{0n-1}=0\ . \quad (45b)$$

The coefficients used in these equations are

$$A_n^{\pm}=v_0^2(n+1)\frac{2b(2n+1)+\Gamma}{[b(2n+1)+\Gamma/2]^2+(\Delta\mp\omega_z)^2}\ ,$$
$$B_n^{\pm}=v_0^2(n+1)\frac{3b(2n+1)+3\Gamma/2\pm 3i\omega_z+i\Delta}{[b(2n+1)+\Gamma/2\pm i\omega_z]^2+\Delta^2}\ ,$$
$$C_n^{\pm}=v_0^2(n+1)\frac{2b(2n+1)+\Gamma\pm 2i\omega_z}{[b(2n+1)+\Gamma/2\pm i\omega_z]^2+\Delta^2}\ , \quad (46)$$
$$D_n^{\pm}=v_0^2(n+1)\frac{1}{b(2n+1)+\Gamma/2-i(\Delta\mp\omega_z)}\ .$$

If now one defines the column vector

$$x^{0n}=(w_{+}^{0n},w_{-}^{0n},w_{+-}^{0n},w_{-+}^{0n})^T \quad (47)$$

one has again a (complex) matrix recursion relation of the form (37).

V. COMPARISON WITH PREVIOUS ANALYTIC RESULTS FOR PDM LASER EXCITATION

The two lowest-order terms in the continued-fraction expansion for the BMPDM are physically significant. The Hanle signal for monochromatic light is given by the lowest-order result, $w_0=A^{-1}y_0$, where A is defined by (22) and (9). The next term, taken in the limit $\beta\to\infty$, reduces to the result obtainable from Burshtein's phase-jump model[20] or from Wiener-Levy phase-diffusion process. This may be shown as follows. From (9), (36), (37), (A1), and (A2) for $n=0$, we have

$$x_0=(A+z_0Bx_1x_0^{-1})^{-1} \quad (48)$$

and from (32) and (A4) for $n=1$

$$x_1x_0^{-1}=-(A+\beta+\sqrt{2}z_0Bx_2x_1^{-1})^{-1}z_0B$$
$$\to\left[-\left[\frac{b}{\beta}\right]^{1/2}B\right]_{\beta\to\infty}\ . \quad (49)$$

From the BMPDM density-matrix equations, one can deduce that $B^2=-D$, where D is a diagonal matrix with $D_{ii}=0$ for $i=1-4$, and $D_{ii}=1$ for $i=5-8$. Furthermore, in the limit $\beta\to\infty$, $b=\Delta\omega_L/2$. Using also $z_0^2=b\beta$ from (32), the density-matrix equations reduce to

$$w_0=(A+D\Delta\omega_L/2)^{-1}y_0\ . \quad (50)$$

Taking diagonal elements of A from (9) and (22), one finds that the optical coherence elements ψ_i $i=5-8$ in Eq. (8) relax at the rate $(\Gamma+\Delta\omega_L)/2$. This conclusion agrees with the substitution rule for optical-absorption processes found by Eberly[44] for the Wiener-Levy phase diffusing field ($\beta\to\infty$, Lorentzian laser spectral profile). The same distribution rule can also be obtained from a comparison of Burshtein's equations for the phase-jump model[20] with the standard Bloch equations for a two-level atom.[40]

The Hanle signal is $S=\psi_1+\psi_2-\psi_3$ in terms of the ψ_i defined by Eq. (8). For the case of zero detuning, $\Delta=0$, a relatively simple analytic expression may be obtained from (9), (37), and (50). We define $\gamma=\Delta\omega_L/\Gamma$, and obtain

$$S=\frac{2v^2\omega_z^2(2+\gamma)}{Q+R} \quad (51)$$

where

$$Q=\omega_z^4+4v^4+v^2\omega_z^2(1+3\gamma)\ ,$$
$$R=\frac{\Gamma^2}{4}[\omega_z^2(2+2\gamma+\gamma^2)+5v^2(1+\gamma)]+\frac{\Gamma^4}{16}(1+\gamma)^2\ . \quad (52)$$

Equation (51) with $R=0$ is identical to Eq. (5.5) of Avan and Cohen-Tannoudji[23] when expressed in their parameters, $\omega_1=\sqrt{2}v$, $\Omega_e=\omega_z$, and also taking $T_1=(\Delta\omega_L)^{-1}$. This last substitution is equivalent to taking the limit $\beta=\infty$. In the BMPDM, finite values of β require the full continued-fraction evaluation rather than adjustments to T_1 as in Ref. 23. With $R=0$, terms in Γ are neglected relative to terms in v, so this approximation is valid only in the high-intensity limit.

With the additional term R, Eqs. (51) and (52) give the exact expression for the on-resonance Hanle signal with a $J=0\leftrightarrow J=1$ transition with either monochromatic light ($\gamma=0$) or with a Wiener-Levy phase-diffusion model ($\beta\to\infty$, $\gamma\neq 0$).

VI. RESULTS

Our calculations show that the shape of the Hanle signal is sensitive not only to the intensity and bandwidth of laser exciting light, but also to the type of fluctuations that produces the spectral broadening. Not surprisingly, the sensitivity to laser characteristics increases with laser intensity.

In the following discussion, all results are presented in terms of scaled parameters. Laser intensities are expressed in terms of a scaled Rabi frequency $\omega_S=\tau\omega_R$ or its rms average, where ω_R is defined in (5). Often one defines a saturation parameter, $S=2\tau^2\omega_R^2$. Hence

$\omega_S = \sqrt{S/2}$. The scale unit for magnetic field is the traditional Hanle half-width at half maximum with broadband excitation, $B^{\infty}_{1/2} = \hbar/2g\mu_0\tau$. Also, laser widths will always be scaled by the natural linewidth of the atomic transition, so the width parameter will be $\tau\Delta\omega_L = \Delta\omega_L/\Gamma$. For experiments on the Yb 556-nm line, $S=1$ corresponds to 0.14 mW/cm^2, $B^{\infty}_{1/2} = 44$ μT, and $\Gamma = 0.18$ MHz. In contrast to the experimental results in Ref. 5, in the computational results presented here there is no averaging over a Doppler distribution of resonance frequencies.

A. Phase-diffusion model

Typical curves for fluorescence intensity versus magnetic field calculated for the Hanle effect by methods discussed above are shown in Fig. 4. The curves at the top show signals for phase diffusing laser light with a near Lorentzian spectral profile, while those in the bottom part were calculated for a nearly Gaussian profile, in each case with a laser spectral width $\Delta\omega_L = 5\Gamma$. With a given laser spectral width, the Hanle dip width increases with laser intensity, and this increase is more rapid if the profile is more nearly Gaussian, as discussed previously.[5,23] Note also that the falloff in the wings is steeper if the exciting light has a more nearly Gaussian profile. (Figure 11 of Ref. 5 shows an experimental observation of this effect.)

The variation of the width of the Hanle dip with laser intensity, bandwidth, and spectral shape can be displayed more directly with plots of the Hanle half width at half maximum (HWHM), as displayed in Fig. 5 for several values of the laser spectral width for a Lorentzian profile. With purely monochromatic light, the Hanle zero-field dip broadens as the square root of laser intensity (linearly with Rabi frequency). This may be attributed to partial

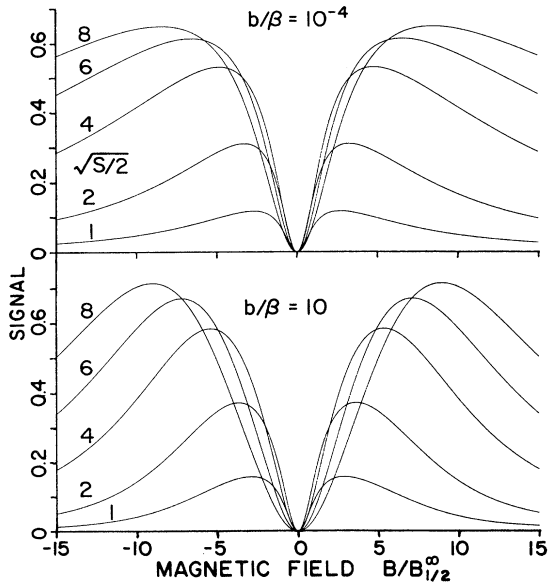

FIG. 4. Typical Hanle fluorescence signals vs magnetic field calculated with the BMPDM for laser bandwidth $\Delta\omega_L = 5\Gamma$, with scaled Rabi frequencies as indicated. Near Lorentzian spectral profile at top, near Gaussian profile at bottom.

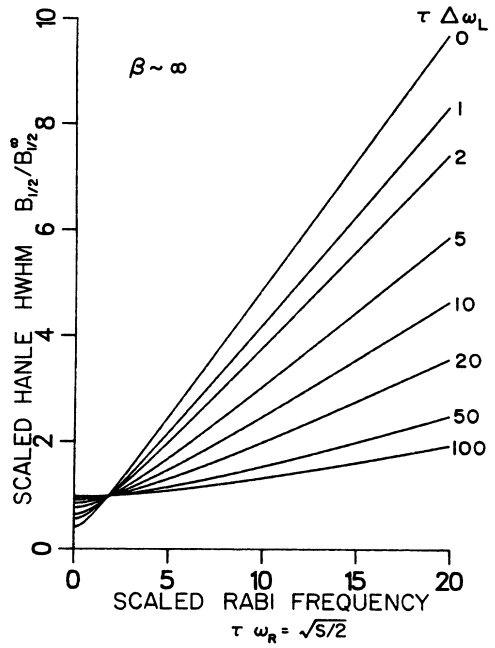

FIG. 5. Calculated scaled Hanle HWHM vs scaled Rabi frequency for PDM laser excitation in the pure Lorentz limit ($\beta \to \infty$), for scaled laser bandwidth as indicated.

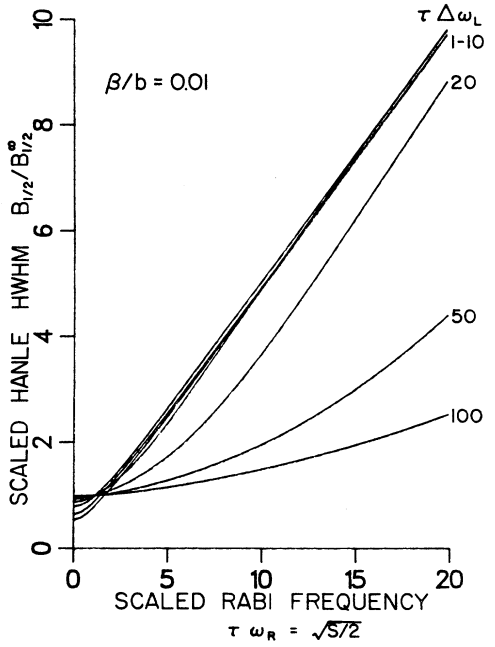

FIG. 6. Calculated scaled Hanle HWHM vs scaled Rabi frequency for PDM laser excitation close to the Gaussian limit for scaled laser width values as indicated.

preservation of the coherence between $m_J=\pm 1$ upper state sublevels by stimulated excitation and deexcitation by the laser light in the presence of the magnetic field. When the laser phase fluctuates, the ± 1 sublevel coherence is maintained less effectively, and broadening decreases. Alternatively, when the laser spectral width increases, there is less intensity within the full width at half maximum (FWHM) of the atomic transition, hence less broadening. Experimental data (Fig. 9 of Ref. 5) from the Yb 556-nm line for laser light with a Lorentzian profile have demonstrated the decrease in power broadening of the Hanle dip with increasing laser spectral width.

Figure 6 presents results for a nearly Gaussian spectral profile analogous to the results for pure Lorentzian profile of Fig. 5. The concentration of intensity within the half-maximum points results in power broadening that is nearly constant even as the laser spectral width increases to ten times the natural width of the atomic transition. Eventually as the Gaussian profile becomes even broader, the broadening of the Hanle dip does diminish.

The variation of Hanle HWHM with laser width for various intensities and ratios of b/β is shown in Fig. 7. For low intensities, the Hanle dip is narrower for monochromatic light than for white light. This may be attributed to the signal falloff at high magnetic field due to detuning, and was observed experimentally by Rasmussen, Schieder, and Walther[16] and obtained theoretically by Avan and Cohen-Tannoudji.[15] The powder broadening at higher intensities decreases when the laser spectral width becomes greater than the power broadened atomic linewidth. However, if the laser spectral shape is sufficiently Gaussian (b/β is large enough), there is a regime in which the Hanle HWHM increases as laser bandwidth increases, just as for the low-intensity case. Here too, as $\Delta\omega_L$ increases up to several times Γ, the relative falloff of intensity in the wings at high field is more significant than the small increase in power broadening.

In the report of experimental work by Arnett *et al.*,[5] incipient effects of large b/β are shown in their Fig. 12. Hanle signals with $b/\beta=4.0$ exhibited about 25% more power broadening than those with $b/\beta=0.75$ for $S\equiv 100-400$. To consider the full range of effects of large b/β, we plot Hanle HWHM versus β in Fig. 8 for two intensity values and several bandwidths. For a narrow-band laser ($\tau\Delta\omega_L=0.2$ here), the Hanle HWHM is essentially the same in the Lorentzian (large β) and Gaussian (small β) limits. However, when the bandwidth $\tau\Delta\omega_L$ is as large as 20, the Hanle HWHM varies by nearly a factor of 3 between the two limits if the scaled Rabi frequency, ω_S is 16, and almost a factor of 2 when $\omega_S=4$. The Hanle HWHM is more sensitive to β if the intensity is greater or the bandwidth is larger. Note also that the effects of increasing or diminishing β eventually do saturate.

If laser excitation of Hanle signals is not at the zero-field resonance frequency, some quite different shape effects occur. Figure 9 shows a number of curves for low (left side) and high (right) intensity, with both Lorentzian (top) and Gaussian (bottom) profile. In each case the detuning is 10Γ, equivalent to 20 times $B_{1/2}^{\infty}$. The signal is always zero for $B=0$, and a recognizable dip occurs at $B=0$ if there is enough intensity in the wings from power broadening, from the laser spectral width, or even from

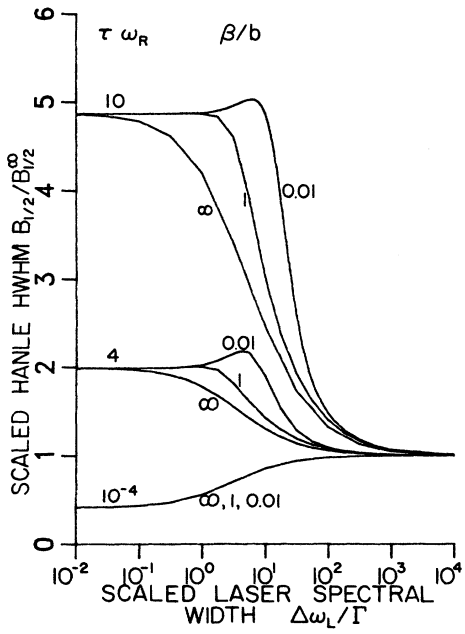

FIG. 7. Calculated scaled Hanle HWHM vs scaled laser spectral width with the BMPDM for scaled Rabi frequency and β/b ratios as indicated.

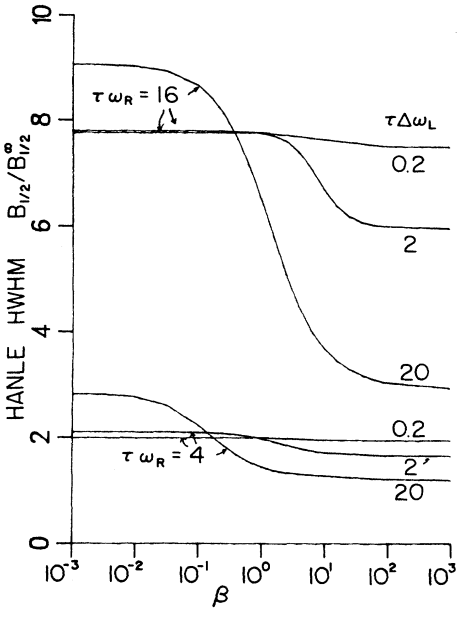

FIG. 8. Calculated scaled Hanle HWHM vs $\log_{10}(\beta)$ for scaled Rabi frequency equal to 16 and 4, for three values of the laser bandwidth.

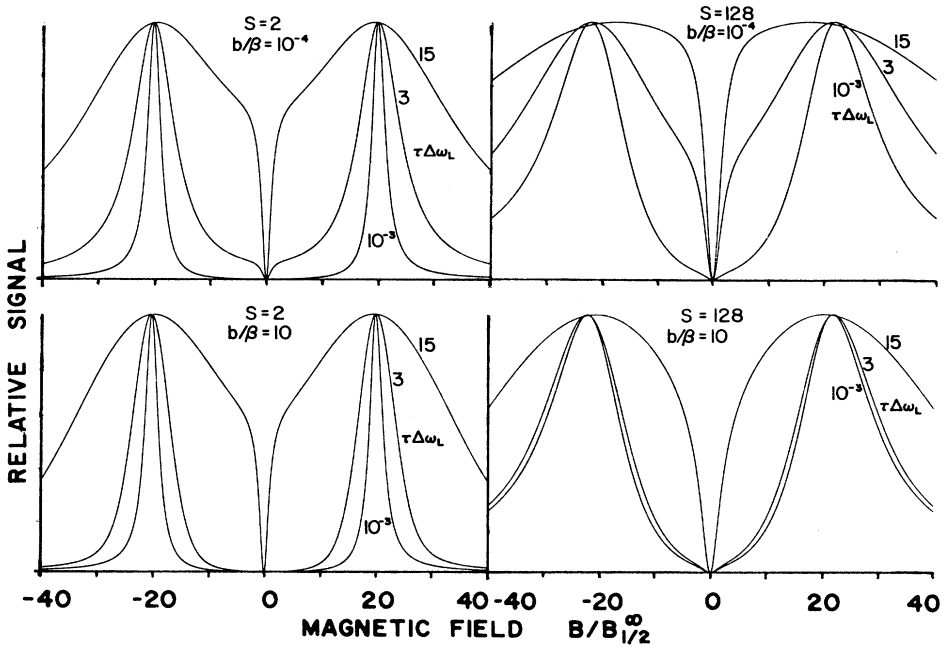

FIG. 9. Hanle fluorescence signal vs magnetic field with the laser center frequency detuned by 10Γ, for two intensity levels, two ratios of b/β, and three laser spectral bandwidths as indicated.

Doppler broadening, as shown in Fig. 13 of Ref. 5. At relatively high intensity (right side of Fig. 9), the Hanle curves with detuned laser are particularly sensitive to the laser spectral profile.

B. Gaussian amplitude model

Calculated Hanle widths for Gaussian amplitude fluctuations of the laser field show an immediate contrast with the results from the phase-diffusion model. Even in the monochromatic limit, which implies long coherence time, there is a Gaussian distribution of field amplitudes. The Hanle HWHM signal in the limit of infinitely narrow laser width is thus equivalent to averaging Hanle signals with monochromatic light [as given by Eqs. (51) and (52) with $\gamma=0$] over the amplitude distribution, and consequently results in a Hanle width less than one-half that obtained with purely monochromatic nonstochastic light with the same mean intensity (same rms Rabi frequency). Figure 10, when compared with Fig. 6, shows this contrast clearly (note that the vertical scales differ in the two figures). The dependence of Hanle HWHM with rms Rabi frequency is essentially linear in the monochromatic limit, but when the laser width is equal to the atomic linewidth, the Hanle HWHM varies nearly as the square root of the Rabi frequency. We have no simple explanation for this rather surprising result. For larger laser widths, Fig. 10 shows that the GAM gives again a roughly linear dependence of the Hanle FWHM with Rabi frequency.

C. Chaotic field model

A plot of Hanle HWHM values for the chaotic field over a range of bandwidths is given in Fig. 11. For the

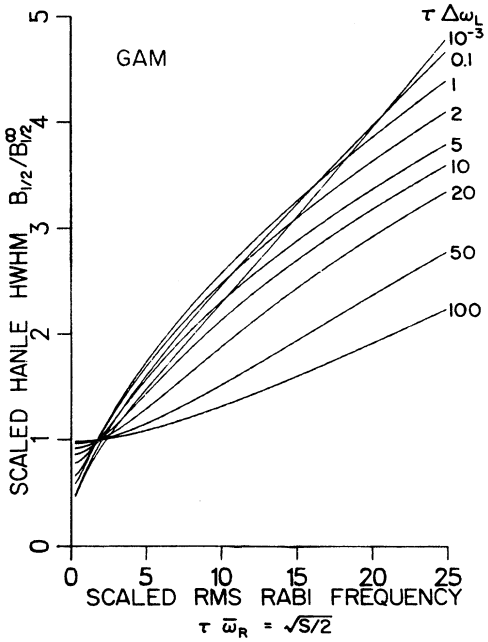

FIG. 10. Calculated scaled Hanle HWHM vs scaled rms Rabi frequency for the GAM, for laser scaled spectral bandwidths as indicated.

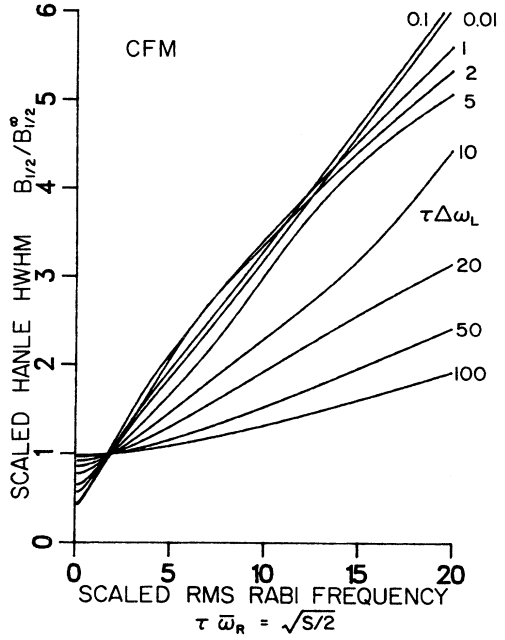

FIG. 11. Calculated scaled Hanle HWHM vs scaled rms Rabi frequency for the CFM, for laser scaled spectral bandwidths as indicated. Note that the HWHM does not vary monotonically with laser bandwidth.

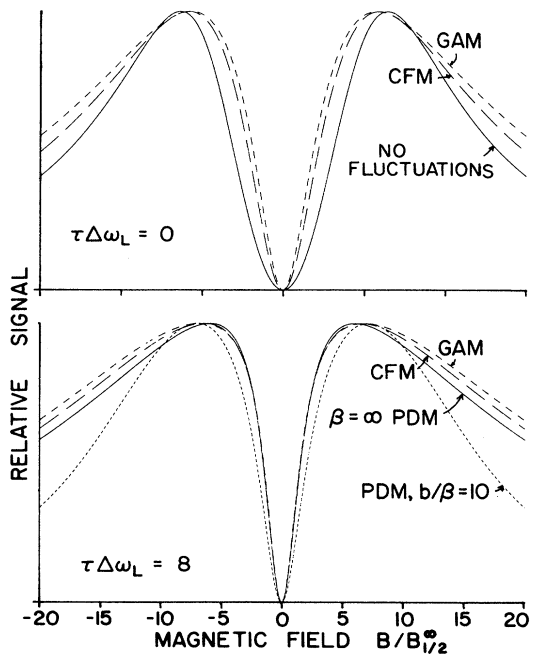

FIG. 12. A comparison of Hanle line shapes for the different fluctuating models, and two laser bandwidths, as indicated. The scaled Rabi frequency $\tau\omega_R = 8$ in every case.

CFM, the monochromatic limit is equivalent to averaging Eq. (52) with $\gamma = 0$ over the field amplitude distribution given by Eq. (20). This results in Hanle signals with dip widths intermediate between the PDM and the GAM. At a scaled rms Rabi frequency of 20, the scaled Hanle HWHM values for the nonstochastic monochromatic field, the CFM, and the GAM are 9.70, 6.05, and 3.93, respectively, so the effect of averaging over field amplitude is clearly significant. With the CFM, there is only a small probability that both the real and imaginary parts of the amplitude will be near zero, and thus the excursions of the field amplitude are smaller than with the GAM.

The curves for the CFM in Fig. 11 are particularly nonlinear and nonmonotonic with scaled bandwidth. However, as in almost all cases, for a scaled Rabi frequency of about 1.8, the scaled HWHM values cross at the value near unity. Some of the more subtle features of these curves will no doubt be lost if there is a Doppler spread of resonance frequencies with a width appreciably greater than Γ.

D. A comparison of line shapes

In view of the contrasting results for the Hanle HWHM from the PDM, GAM, and CFM, even in the limit of monochromatic light, a comparison of line shapes is clearly of interest. Figure 12 (top) shows calculated Hanle signals with three species of monochromatic light, normalized to a constant peak signal. Averaging over a distribution of amplitudes flattens the peak, hence narrows the Hanle dip and broadens the wings. Figure 12 (bottom) shows that when the laser width is greater (8Γ in this case), all three Lorentz profiles, GAM, CFM, and BMPDM with $\beta = \infty$ give very similar shapes. However, the BMPDM Gaussian profile does show appreciably more broadening of the Hanle dip and more rapid falloff in the wings.

VII. DISCUSSION AND CONCLUSION

The formalism presented here shows that methods developed primarily by Zoller and co-workers for stochastic density-matrix equations can be extended to multilevel atom transitions. Previously,[6–11] the BMPDM, GAM, and CFM have been applied basically to two-level processes, possibly coupled to additional levels by weak, nonstochastic probe fields. For the BMPDM and GAM, the approach discussed here has been to define real variables and avoid the algebra required for the "top-down" evaluation of continued fractions. In preliminary work, we have also pursued the alternative approach which involves algebraic elimination of four variables, but the expressions are more complicated to present and more susceptibile to errors, and the added efficiency in the continued-fraction expansion not compelling. However, with the CFM it is necessary to perform the algebraic elimination to reduce the problem to four (complex) variables.

The computational results presented here show that laser-excited Hanle-effect signal shapes are sensitive not only to laser intensity and bandwidth, but also the nature of fluctuations. We have been concerned primarily with

the zero-field coherence dip because it reflects the coherence between the excited-state sublevels. One could also examine the "outer" HWHM, considering the point at which the Hanle signal falls to one-half its maximum value at higher magnetic fields due to detuning. This quantity is less interesting because it reflects the spectral distribution of the laser light and the power broadening in much the same manner as the width of a two-level atom transition as a function of detuning. Also in experiments, the "outer" HWHM will be more sensitive to the Doppler distribution of the atoms than the "inner" HWHM discussed here.

Very ingenious and elaborate schemes[1,2,12] have been developed to produce laser fields that closely follow the idealized models discussed here. Precise comparisons with experiment will be conditioned by several factors, such as possible variation of laser intensity over the interaction region and averaging over a Doppler distribution of resonant frequencies, as discussed by Arnett *et al.*[5]

A more intractable limitation on the experiments occurs because there happens to be very few atomic transitions at a convenient wavelength in which the ground state is $J=0$ and the excited state $J=1$ with no hyperfine structure.[5] Extension of the theoretical results to transitions of higher J or F value will involve larger matrices in the continued-fraction expansions. For example, for $F=3\leftrightarrow F=4$ transitions, as occur in Rb or Cs D line hyperfine components, there will be 16^2-1 density-matrix elements rather than 3^2-1 here. Furthermore, there will be complications due to the redistribution of population by spontaneous decay to different ground-state sublevels and due to optical pumping effects. Typically, spontaneous decay to other hyperfine levels will also occur. The Hanle effect in forward scattering of nonfluctuating laser light has been studied for transitions of higher J,[45] and the next simplest case, with ground state $J=1$ and upper state $J=0$, is now being pursued experimentally with fluctuating laser light.[46]

Experimental techniques do exist for narrowing both dye and diode lasers to the kHz regime, narrow enough to be considered effectively monochromatic for typical allowed atomic transitions at optical frequencies. However, often in designing an experiment or analyzing results, it is useful to know what effects can occur with finite-bandwidth excitation.

ACKNOWLEDGMENTS

Experimental work by H. J. Metcalf, S. J. Smith, and D. S. Elliott and co-workers has provided the motivation for this study, and we thank these people for continued interest and encouragement. Also we are pleased to acknowledge useful discussions with P. Zoller, S. Dixit, P. Berman, and S.-Q. Shang. This work was supported by the National Science Foundation.

APPENDIX

The time-independent matrix recursion equation (38) may be solved by standard continued-fraction techniques.[41] The "top-down" methods described by Dixit, Zoller, and Lambropoulos[10] may be tested for convergence after each term. For this approach it is necessary to eliminate enough variables that the matrix B in (36), for example, is nonsingular. This algebra can be avoided by retaining all eight variables (for the case discussed here) and evaluating the continued fraction "from the bottom up," in which case B^{-1} does not occur.[47] It is then necessary to test convergence by starting over at a higher value of $n_{\max}$, but when scanning the magnetic field with the Hanle effect, usually only one or two test values of $n_{\max}$ are necessary at each field value. The following computational procedure is applicable to equations of the form (37).

In Eq. (37), we define

$$w_n = x_n y_0 \tag{A1}$$

so that the matrix recursion relation becomes

$$c_n x_n + d_n x_{n+1} + d_{n-1} x_{n-1} = \delta_{n0} \ . \tag{A2}$$

From the equation for $n=0$,

$$x_0 = (c_0 + d_0 x_1 x_0^{-1})^{-1} \ . \tag{A3}$$

For arbitrary n,

$$x_n x_{n-1}^{-1} = -(c_n + d_n x_{n+1} x_n^{-1})^{-1} d_{n-1} \ . \tag{A4}$$

This recursion relation may be evaluated "from the top down" by setting

$$s_n = -d_n c_{n+1}^{-1} d_n \tag{A5}$$

for some maximum value of n, and then using recursively

$$s_{n-1} = -d_{n-1}(c_n + s_n)^{-1} d_{n-1} \tag{A6}$$

down to s_0. Finally,

$$w_0 = (c_0 - s_0)^{-1} y_0 \ . \tag{A7}$$

---

*Also at Grumman Corporate Research Center, Bethpage, NY 11714.

[1]D. S. Elliott, R. Roy, and S. J. Smith, Phys. Rev. A **26**, 12 (1982).

[2]D. S. Elliott and S. J. Smith, J. Opt. Soc. B **5**, 1927 (1988).

[3]M. Hamilton, D. S. Elliott, K. Arnett, and S. J. Smith, Phys. Rev. A **33**, 778 (1986); M. Hamilton, K. Arnett, S. J. Smith, D. S. Elliott, M. Dziemballa, and P. Zoller, *ibid.* **36**, 178 (1987).

[4]D. S. Elliott, M. W. Hamilton, K. Arnett, and S. J. Smith, Phys. Rev. Lett. **53**, 439 (1984); Phys. Rev. A **32**, 887 (1985).

[5]K. Arnett, S. J. Smith, R. E. Ryan, T. Bergeman, H. Metcalf, M. Hamilton, and J. Brandenberger, Phys. Rev. A **41**, 2580 (1990).

[6]P. Zoller and F. Ehlotzky, J. Phys. B **10**, 3023 (1977); P. Zoller, *ibid.* **10**, L321 (1977); **11**, 805 (1978); P. Zoller and P. Lambro-

poulos, *ibid.*, **12**, L547 (1979).
[7]P. Zoller, Phys. Rev. A **19**, 1151 (1979).
[8]P. Zoller, Phys. Rev. A **20**, 1019 (1979).
[9]P. Zoller, G. Alber, and R. Salvador, Phys. Rev. A **24**, 398 (1981).
[10]S. Dixit, P. Zoller, and P. Lambropoulos, Phys. Rev. A **21**, 1289 (1975).
[11]A. T. Georges, Phys. Rev. A **21**, 2034 (1980).
[12]C. Xie, G. Klimeck, and D. S. Elliott, Phys. Rev. A **41**, 6376 (1990).
[13]D. S. Elliott (private communication).
[14]W. Hanle, Z. Phys. **30**, 93 (1924).
[15]P. Avan and C. Cohen-Tannoudji, J. Phys. (Paris) Lett. **36**, L85 (1975).
[16]W. Rasmussen, R. Schieder, and H. Walther, Opt. Commun. **12**, 315 (1974).
[17]A. T. Georges, P. Lambropoulos, and P. Zoller, in *Laser Spectroscopy IV,* edited by H. Walther and K. Rothe (Springer, Berlin, 1977).
[18]R. Boscaino and R. Mantegna, Phys. Rev. A **40**, 5 (1989).
[19]M. Anderson, R. Jones, S. J. Smith, D. Elliott, H. Ritsch, and P. Zoller, Phys. Rev. Lett. **64**, 1346 (1990).
[20]A. Burshtein, Zh. Eksp. Teor. Fiz. **48**, 850 (1964) [Sov. Phys.—JETP **21**, 567 (1965)].
[21]G. S. Agarwal, Phys. Rev. A **18**, 1490 (1978).
[22]P. Avan and C. Cohen-Tannoudji, J. Phys. B **10**, 155 (1977).
[23]P. Avan and C. Cohen-Tannoudji, J. Phys. B **10**, 171 (1977).
[24]K. Wodkiewicz, and J. Eberly, Phys. Rev. A **32**, 992 (1985).
[25]M. W. Hamilton (unpublished).
[26]R. Boscaino and R. Mantegna, Phys. Rev. A **40**, 13 (1989).
[27]A. Kofmann, R. Zaibel, A. Levine, and Y. Prior, Phys. Rev. A **41**, 6434 (1990); **41**, 6454 (1990).
[28]H. Ritsch, P. Zoller, and J. Cooper, Phys. Rev. A **41**, 2653 (1990).
[29]G. Vemuri, R. Roy, and G. Agarwal, Phys. Rev. A **41**, 2749 (1990).
[30]M. Lax, Phys. Rev. **157**, 213 (1967); **160**, 290 (1967).
[31]H. Haken, *Laser Theory* (Springer, Berlin, 1970).
[32]A. L. Schawlow and C. H. Townes, Phys. Rev. **112**, 1940 (1958).
[33]C. H. Henry, IEEE J. Quantum Electron **18**, 259 (1982); **19**, 1391 (1983).
[34]H. Gerhardt, H. Welling, and A. Guttner, Z. Phys. **253**, 113 (1972).
[35]P. Milonni and J. Eberly, *Lasers* (Wiley, New York, 1988).
[36]A. Mooradian, Phys. Today **38** (5), 43 (1985); K. Kikuchi, IEEE J. Quantum Electron. **QE-25**, 684 (1989).
[37]G. P. Agrawal and R. Roy, Phys. Rev. A **37**, 2495 (1988).
[38]A. Papoulis, *Probability, Random Variables, and Stochastic Processes* (McGraw-Hill, New York, 1965).
[39]G. E. Uhlenbeck and L. S. Ornstein, Phys. Rev. **36**, 823 (1930).
[40]S. Stenholm, *Foundations of Laser Spectroscopy* (Wiley, New York, 1984).
[41]H. Risken, *The Fokker-Planck Equation* (Springer, Berlin, 1989).
[42]N. G. van Kampen, *Stochastic Processes in Physics and Chemistry* (North-Holland Elsevier, Amsterdam, 1981).
[43]See, for example, J. W. Goodman, *Statistical Optics* (Wiley, New York, 1985).
[44]J. H. Eberly, Phys. Rev. Lett. **37**, 1387 (1976); and in *Laser Spectroscopy IV,* Ref. 17.
[45]B. Stahlberg, M. Lindberg, and P. Junger, J. Phys. B **18**, 627 (1985); P. Junger, T. Fellman, B. Stahlberg, and M. Lindberg, Opt. Commun. **73**, 38 (1989).
[46]M. W. Hamilton (private communication).
[47]See the Appendix of Ref. 10 and pp. 226–226 of Ref. 41.